JOC The Journal of Organic Chemistry

Article

pubs.acs.org/joc

Sphenostylisins A–K: Bioactive Modified Isoflavonoid Constituents of the Root Bark of *Sphenostylis marginata* ssp. *erecta*

Jie Li,[†] Li Pan,[†] Ye Deng,[†] Ulyana Muñoz-Acuña,[†,‡] Chunhua Yuan,[§] Hongshan Lai,[†] Heebyung Chai,[†] Tangai E. Chagwedera,[∥] Norman R. Farnsworth,[⊥,#] Esperanza J. Carcache de Blanco,[†,‡] Chenglong Li,[†] Djaja D. Soejarto,[⊥,¶] and A. Douglas Kinghorn*[,†]

[†]Division of Medicinal Chemistry and Pharmacognosy, College of Pharmacy, The Ohio State University, 500 West 12th Avenue, Columbus, Ohio 43210, United States

[‡]Division of Pharmacy Practice and Administration, College of Pharmacy, The Ohio State University, 500 West 12th Avenue, Columbus, Ohio 43210, United States

[§]Nuclear Magnetic Resonance Facility, Campus Chemical Instrument Center, The Ohio State University, Columbus, Ohio 43210, United States

[∥]Department of Pharmacy, University of Zimbabwe, Harare, Zimbabwe

[⊥]Department of Medicinal Chemistry and Pharmacognosy, College of Pharmacy, University of Illinois at Chicago, Chicago, Illinois 60612, United States

[¶]Field Museum of Natural History, Chicago, Illinois 60605, United States

Supporting Information

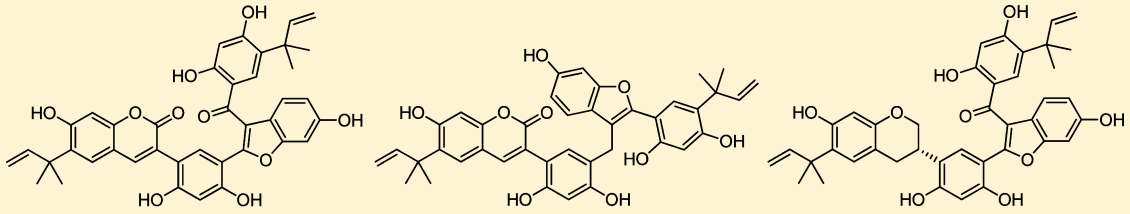

Sphenostylisin A (**1**)
NF-κB inhibition: IC_{50} = 6 nM

Sphenostylisin B (**2**)

Sphenostylisin C (**3**)

ABSTRACT: Sphenostylisins A–C (**1**–**3**), three complex dimeric compounds representing two novel carbon skeletons, along with an additional eight new compounds, sphenostylisins D–K (**4**–**11**), were isolated from the active chloroform-soluble extract of the root bark of *Sphenostylis marginata* ssp. *erecta* using a bioactivity-guided isolation approach. The structures were elucidated by means of detailed spectroscopic analysis, including NMR and HRESIMS analysis, and tandem MS fragmentation was utilized to further support the structures of **1**–**3**. The absolute configuration of sphenostylisin C (**3**) was established by electronic circular dichroism analysis. Plausible biogenetic relationships between the modified isoflavonoids **1**–**11** are proposed, and a cyclization reaction of **9** was conducted to support one of the biogenetic proposals made. All of these pure isolates were evaluated against a panel of in vitro bioassays, and among the results obtained, sphenostylisin A (**1**) was found to be a very potent NF-κB inhibitor (IC_{50} = 6 nM).

INTRODUCTION

Sphenostylis marginata E. Mey. ssp. *erecta* (Baker f.) Verdc. [syn.: *Dolichos erectus* Baker f.; *Sphenostylis erecta* (Baker f.) Hutch. ex Baker f.; Fabaceae; African yellow pea), is a medicinal plant used as an antiseptic and for the treatment of abdominal pain, diarrhea, edema, and fever.[1] In addition, the edible tubers, flowers, and starchy fruits of *S. marginata* are utilized as a food source in some African countries.[2] Although the carbohydrate, amino acid, and protein composition profiles of *Sphenostylis* species have been studied previously,[2] there has been only one reported study of secondary metabolites: four antifungal pterocarpans isolated from the root bark of *S. marginata* ssp. *erecta*.[3]

Scavenging of reactive oxygen species by antioxidants and enhancement of carcinogen detoxification via induction of phase-II enzymes such as quinone reductase (QR) are two important cancer chemopreventive strategies, while inhibition of nuclear factor kappa B (NF-κB) is a promising approach for both cancer chemotherapy and chemoprevention.[4,5] In our search for naturally occurring compounds that combat cancer, we found that the chloroform-soluble extract of the root bark of *S. marginata* ssp. *erecta* collected in Zimbabwe showed both hydroxyl radical-scavenging and QR-inducing activities. Assays

Received: July 19, 2013
Published: September 17, 2013

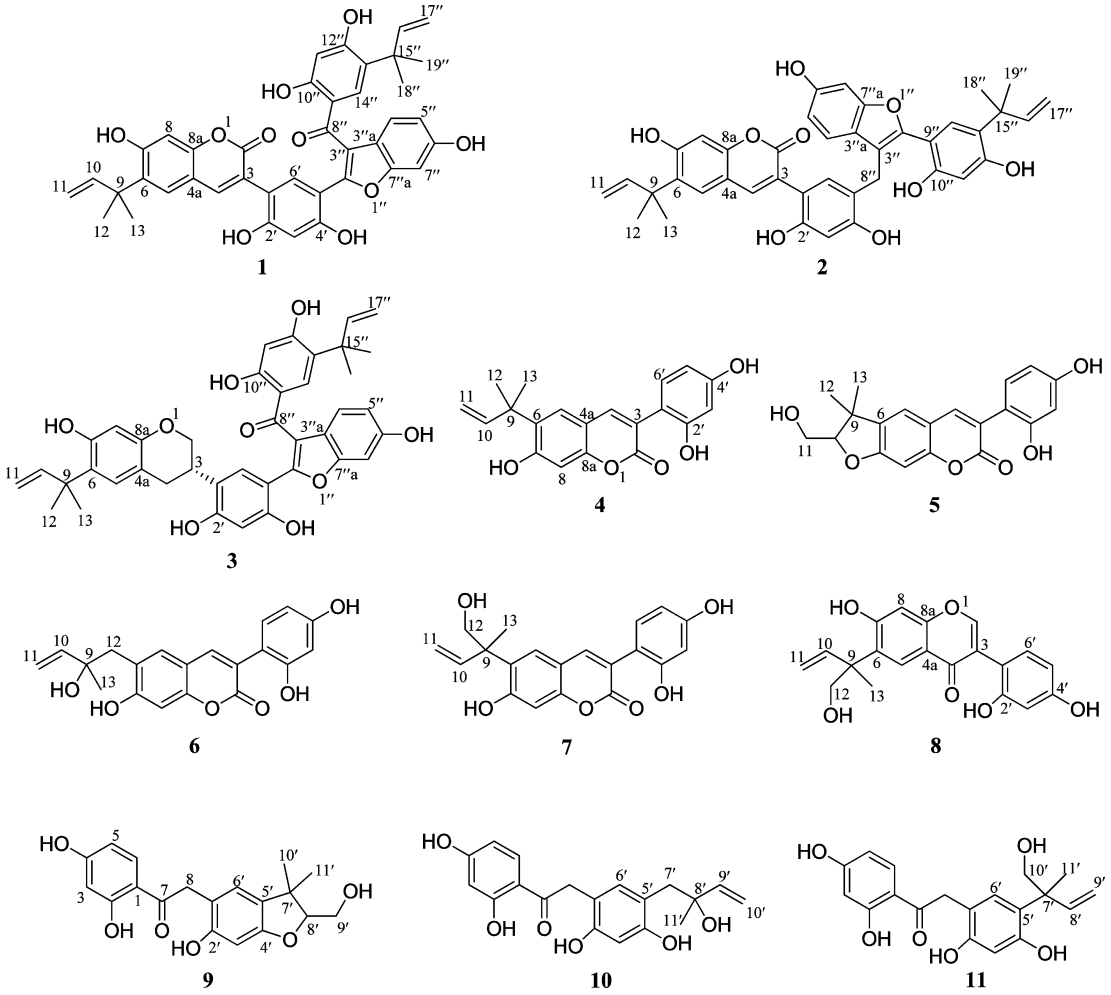

Figure 1. Structures of the new compounds isolated from *S. marginata* ssp. *erecta*.

that measured these two activities were used in tandem to guide compound isolation. Herein we report the isolation and structure elucidation of sphenostylisins A–C (**1**–**3**), representative of two novel carbon skeletons, and an additional eight new compounds, sphenostylisins D–K (**4**–**11**), as well as the biological evaluation of all isolates obtained using the hydroxyl radical-scavenging, QR-inducing, and NF-κB inhibition assays. Compounds **1**–**11** (Figure 1) were also evaluated for their cytotoxicity against the HT-29 human colon cancer cell line.

RESULTS AND DISCUSSION

The methanol extract of the root bark of *S. marginata* ssp. *erecta* was suspended in H_2O and then partitioned sequentially with hexanes, $CHCl_3$, EtOAc, and *n*-BuOH. All of the partitions obtained were evaluated in the in vitro hydroxyl radical-scavenging and QR-inducing assays, and the activities are presented as ED_{50} (test concentration scavenging hydroxyl radicals by 50%) and CD (test concentration that doubles the QR activity) values, respectively. Among these partitions, the $CHCl_3$ partition exhibited the most potent activity in both the hydroxyl radical-scavenging (ED_{50} = 3.3 μg/mL) and QR-inducing (CD = 9.6 μg/mL) assays. Therefore, it was selected for further purification and afforded 11 major fractions. Fraction F05 was active in the hydroxyl radical-scavenging and QR-inducing assays, with ED_{50} and CD values of 1.7 and 5.2 μg/mL, respectively. Accordingly, fraction F05 was subsequently fractionated, leading to the isolation of 11 new modified isoflavonoids, sphenostylisins A–K (**1**–**11**), comprising three complex dimeric compounds representative of two novel carbon skeletons, four 3-phenylcoumarins, three deoxybenzoins, and one isoflavone.

The molecular formula of sphenostylisin A (**1**) was determined to be $C_{40}H_{34}O_{10}$ on the basis of the sodiated molecular ion peak at *m*/*z* 697.2035 (calcd 697.2050) in the HRESIMS spectrum. The analysis of the ^{1}H, ^{13}C, DEPT, ^{1}H–^{1}H COSY, ^{1}H–^{13}C HSQC, and HMBC NMR spectra (Table S1 and Figure S1 in the Supporting Information) suggested that the molecule of **1** has two moieties (fragments A and B), each including a 15-carbon skeleton with an α,α-dimethylallyl side chain. In the ^{1}H NMR spectrum, fragment A showed five aromatic singlets at δ_H 7.73 (1H, H-4), 7.52 (1H, H-6′), 7.46 (1H, H-5), 6.77 (1H, H-8), and 6.35 (1H, H-3′) (Table 1), of which H-4 at δ_H 7.73 was observed as a characteristic proton signal of a 3-phenylcoumarin skeleton. The ^{1}H NMR spectrum of fragment A also showed three hydroxy group singlets at δ_H 10.53 (1H, OH-7), 10.04 (1H, OH-4′), and 9.85 (1H, OH-2′), while resonances at δ_H 6.26 (1H, dd, *J* = 17.5, 10.7 Hz, H-10), 4.97 (1H, br d, *J* = 10.7 Hz, H-11a), 4.95 (1H, br d, *J* = 17.5 Hz, H-11b), and 1.48 (6H, s, CH_3 × 2, H-12/13) were attributed to an α,α-dimethylallyl side chain. The ^{13}C NMR spectrum of fragment A showed 20 carbon signals, which were classified from the DEPT and

dx.doi.org/10.1021/jo401573h | J. Org. Chem. 2013, 78, 10166–10177

Table 1. ^{1}H and ^{13}C NMR Spectroscopic Data of Compounds 1−3[a]

	1		2		3	
no.	δ_H[b]	δ_C[c]	δ_H[b]	δ_C[c]	δ_H[b]	δ_C[c]
2α		159.9		160.1	3.77, t (9.7)	69.2
2β					4.09, br d, (9.7)	
3		120.4		121.4	3.25, m	31.4
4α	7.73, s	142.2	7.56, s	141.8	2.87, dd (15.1, 11.7)	29.7
4β					2.64, dd (15.1, 3.5)	
4a		111.1		111.0		111.6
5	7.46, s	126.6	7.37, s	126.4	6.81, s	127.7
6		131.6		131.5		126.1
7		159.3		159.3		154.5
OH-7	10.53, s				9.07, s	
8	6.77, s	102.4	6.68, s	102.2	6.24, s	103.4
8a		153.1		153.0		152.6
9		39.9		39.8		39.5
10	6.26, dd (17.5, 10.7)	147.1	6.21, dd (17.5, 10.7)	147.1	6.24, dd (17.5, 10.7)	148.0
11a	4.97, br d (10.7)	110.6	4.93, br d (10.7)	110.5	4.92, br d (17.5)	109.6
11b	4.95, br d (17.5)		4.91, br d (17.5)		4.90, br d (10.7)	
12	1.48, s	26.9	1.43, s	26.9	1.40, s	26.9
13	1.48, s	26.9	1.43, s	26.9	1.40, s	26.9
1′		114.6		113.7		118.6
2′		157.8		153.9		157.8
OH-2′	9.85, s				9.89, s	
3′	6.35, s	102.8	6.41, s	103.9	6.32, s	102.6
4′		155.9		155.5		154.7
OH-4′	10.04, s				9.75, s	
5′		108.4		116.8		108.3
6′	7.52, s	131.7	6.67, s	131.4	7.23, s	128.1
2″		152.2		149.3		153.0
3″		114.0		114.7		113.7
3″a		120.1		121.9		120.1
4″	7.33, d (8.4)	120.6	7.19, d (8.4)	119.8	7.38, d (8.4)	120.4
5″	6.78, dd (8.4, 1.6)	112.7	6.60, dd (8.4, 1.8)	111.0	6.77, dd (8.4, 1.6)	112.6
6″		155.8		154.8		155.7
OH-6″	9.67, s				9.65, s	
7″	6.98, d (1.6)	97.4	6.80, d (1.8)	97.3	6.97, d (1.6)	97.4
7″a		154.2		154.7		154.2
8″		194.7	3.71, s	22.6		194.6
9″		112.9		108.1		112.8
10″		162.5		154.6		162.4
OH-10″	12.66, s				12.64, s	
11″	6.34, s	103.2	6.44, s	102.4	6.29, s	103.1
12″		163.2		157.2		163.0
OH-12″	10.54, s				10.47, s	
13″		125.8		124.7		125.6
14″	7.32, s	131.4	7.01, s	129.5	7.21, s	131.1
15″		39.2		39.4		39.0
16″	5.84, dd (17.5, 10.7)	147.2	6.10, dd (17.5, 10.7)	147.9	5.78, dd (17.5, 10.7)	147.2
17″a	4.74, br d (10.7)	110.2	4.78, br d (17.5)	109.6	4.73, br d (10.7)	110.0
17″b	4.67, br d (17.5)		4.75, br d (10.7)		4.61, br d (17.5)	
18″	1.09, s	26.6	1.27, s	26.7	1.04, s	26.7
19″	1.09, s	26.6	1.27, s	26.7	1.04, s	26.7

[a]NMR data obtained in DMSO-d_6 for **1**−**3**. Assignments are based on $^{1}H-^{1}H$ COSY, HSQC, and HMBC spectroscopic data. [b]Measured at 800 MHz for ^{1}H NMR; presented as δ in ppm, multiplicity (J in Hz). [c]Measured at 150 MHz for ^{13}C NMR; δ in ppm.

HSQC data as two methyl carbons, six quaternary carbons, six tertiary sp^2 carbons, one secondary sp^2 carbon, four oxygen-bearing tertiary sp^2 carbons, and a conjugated lactone carbonyl resonance at δ_C 159.9. The characteristic NMR data of fragment A were comparable to those of known 3-phenylcoumarins [e.g., licoarylcoumarin, licopyranocoumarin, licofuranocoumarin, and glycycoumarin isolated from *Glycyrrhiza* (licorice) species[6]]. The carbon signal at δ_C 159.9 (C-2), attributed to the conjugated lactone carbonyl on the basis of its correlation with H-4 (δ_H 7.73) in the HMBC spectrum (Figure 2), combined with the HMBC correlations of H-6′ to C-3 (δ_C 120.4) and H-4 to C-1′ (δ_C 114.6) confirmed the presumed 3-

dx.doi.org/10.1021/jo401573h | J. Org. Chem. 2013, 78, 10166−10177

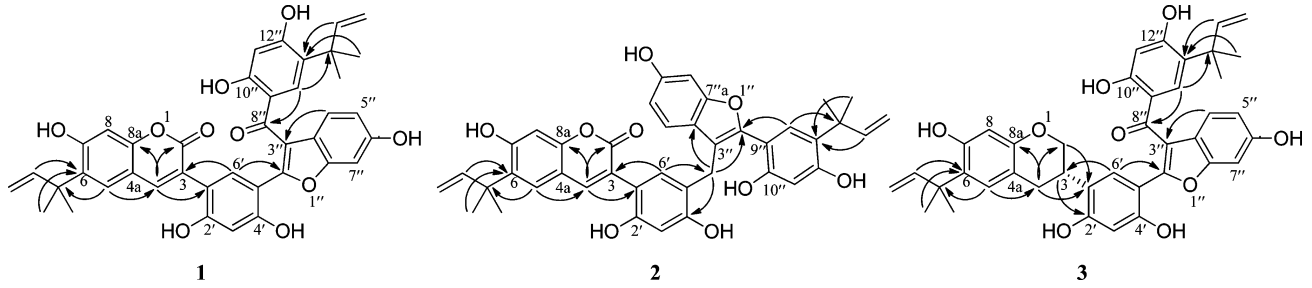

Figure 2. Key HMBC correlations of compounds **1**–**3** with novel carbon skeletons.

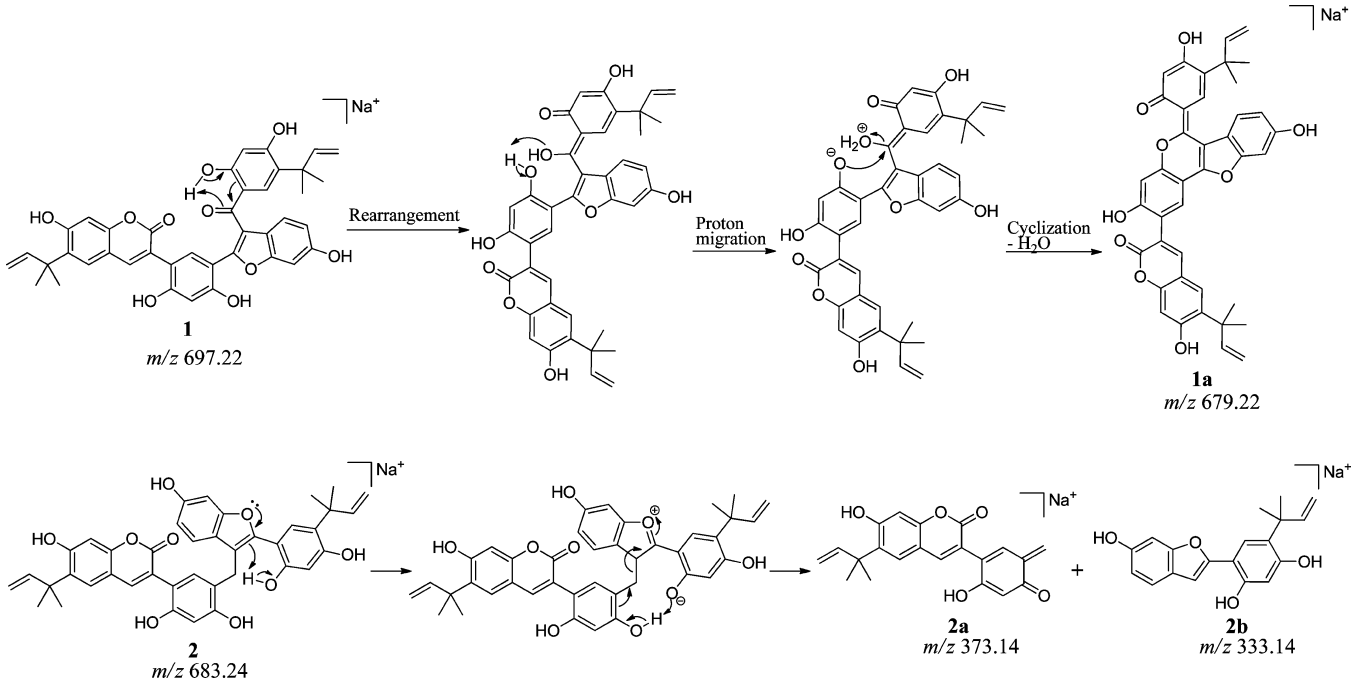

Figure 3. Tandem MS fragmentation pathways of compounds **1** and **2** with novel carbon skeletons.

phenylcoumarin skeleton. Fragment A showed a non-oxygenated signal at C-5 (δ_C 126.6), a position at which most known 3-phenylcoumarins isolated from licorice species have a hydroxy or methoxy group. Thus, a long-range correlation in the HMBC spectrum showed that the proton at δ_H 7.46, attributed to H-5, is correlated with C-4 (δ_C 142.2), C-7 (δ_C 159.3), and C-8a (δ_C 153.1), while the proton at δ_H 6.77 (H-8) is correlated with C-4a (δ_C 111.1) and C-6 (δ_C 131.6). The *α*,*α*-dimethylallyl group was placed at C-6 (δ_C 131.6) on the basis of the HMBC correlations of H-10, H-12, and H-13 to C-6, and this was confirmed by the HMBC cross-peak between H-5 and C-9 (δ_C 39.9). Another key difference is that the 3-phenyl ring of fragment A exhibited only two singlets at δ_H 7.52 (H-6′) and 6.35 (H-3′), which, on comparison to the ABX spin system reported for H-6′, H-5′, and H-3′ in the 3-phenyl ring of known 3-phenylcoumarins isolated from licorice species, indicated that C-5′ is the carbon of attachment to fragment B. The assignments of H-6′ and H-3′ were confirmed from the HMBC correlations of H-6′ to C-2′ (δ_C 157.8) and C-4′ (δ_C 155.9) and of H-3′ to C-1′ (δ_C 114.6) and C-5′ (δ_C 108.4) (Figure 2). When fragment B was considered, observed in the ^{1}H NMR spectrum were signals for three isolated spin systems: a 1,2,4-trisubstituted benzene ring [δ_H 7.33 (1H, d, J = 8.4 Hz, H-4″), 6.98 (1H, d, J = 1.6 Hz, H-7″), and 6.78 (1H, dd, J = 8.4, 1.6 Hz, H-5″)], a 1,2,4,5-tetrasubstituted benzene ring [δ_H 7.32 (1H, s, H-14″) and 6.34 (1H, s, H-11″)], and an *α*,*α*-dimethylallyl group [δ_H 5.84 (1H, dd, J = 17.5, 10.7 Hz, H-16″), 4.74 (1H, br d, J = 10.7 Hz, H-17″a), 4.67 (1H, br d, J = 17.5 Hz, H-17″b), and 1.09 (6H, s, CH_3 × 2, H-18″/19″)]. In addition, there were three hydroxy group singlets at δ_H 12.66 (1H, OH-10″), 10.54 (1H, OH-12″), and 9.67 (1H, OH-6″). The ^{13}C NMR spectrum of fragment B showed 20 carbon signals, including two methyls, five quaternary carbons, six tertiary sp^2 carbons, one secondary sp^2 carbon, five oxygen-bearing tertiary sp^2 carbons, and a carbonyl carbon, as classified from the DEPT and HSQC spectra. The NMR data of fragment B were comparable to those of morachalcone B, a chalcone derivative fused with a furan ring isolated from *Morus alba*.[7] Comparison of the 1D and 2D NMR spectra with those of morachalcone B revealed a major change in the side chain, with a prenyl group in morachalcone B being replaced by an *α*,*α*-dimethylallyl group in fragment B of **1**. The *α*,*α*-dimethylallyl group was determined to be located at C-13″ (δ_C 125.8) according to the HMBC correlations of H-16″, H-18″, and H-19″ to C-13″. The singlet at δ_H 7.32 is correlated with C-8″ (δ_C 194.7), C-10″ (δ_C 162.5), C-12″ (δ_C 163.2), and C-15″ (δ_C 39.2) while the other singlet at δ_H 6.34 is correlated with C-9″ (δ_C 112.9) and C-13″ (δ_C 125.8) in the HMBC spectrum, and thus, these were assigned to H-14″ and H-11″, respectively. The ABX spin system at δ_H 7.33, 6.98, and 6.78

dx.doi.org/10.1021/jo401573h | J. Org. Chem. 2013, 78, 10166–10177

was attributed to H-4″, H-7″, and H-5″ in the benzofuran ring, respectively, on the basis of their splitting pattern and coupling constants, and this was confirmed by the HMBC correlations of H-4″ to C-3″ (δ_C 114.0), C-6″ (δ_C 155.8), and C-7″a (δ_C 154.2); of H-7″ to C-3″a (δ_C 120.1) and C-5″ (δ_C 112.7); and of H-5″ to C-3″a (δ_C 120.1) and C-7″ (δ_C 97.4) (Figure 2). All six hydroxy group proton signals of **1** were also assignable on the basis of their HMBC correlations (Table S1 in the Supporting Information), which facilitated the assignments of the remaining protons and carbons and further supported the structure of **1** as shown. Among these hydroxy group protons, the signal of OH-10″ appeared downfield at δ_H 12.66 as a result of hydrogen bonding with the carbonyl group (C-8″, δ_C 194.7). The connectivity of fragments A and B, determined to be through a carbon−carbon linkage between C-5′ (δ_C 108.4) and C-2″ (δ_C 152.2), was confirmed by direct evidence of a key HMBC correlation between H-6′ and C-2″ (Figure 2 and Figure S1f in the Supporting Information). The structure of **1** elucidated via NMR spectroscopy was supported by the tandem mass spectrum. The highly conjugated structure of **1** did not fragment appreciably through carbon−carbon bond cleavage when collision-induced dissociation (CID) was used, and therefore, only one predominant fragment peak from the parent ion (m/z 697.22 $[M + Na]^+$) was observed at m/z 679.22 $[M + Na - H_2O]^+$ (Figure S13l in the Supporting Information). This may be generated through a proton rearrangement similar to a McLafferty rearrangement, with cyclization occurring to form a stable six-membered ring and the loss of one water molecule[8] (Figure 3). Therefore, the structure of **1** as shown in Figure 1 was elucidated unambiguously. This compound bears a novel carbon skeleton formed through a carbon−carbon bond linkage of a 3-phenylcoumarin skeleton and a 3-arylbenzofuran unit and was accorded the trivial name sphenostylisin A.

Sphenostylisin B (**2**) was determined to have the molecular formula $C_{40}H_{36}O_9$ on the basis of the HRESIMS $[M + Na]^+$ ion peak at m/z 683.2269 (calcd 683.2257), representing one degree of unsaturation less than in compound **1**. The ^1H and ^{13}C NMR spectra of **2** were very similar to those of compound **1** (Table 1). On comparison of the ^1H NMR data of these two compounds, an additional methylene resonance appeared at δ_H 3.71 (2H, s, H-8″) in compound **2**. Correspondingly, an additional carbon signal, classified as a methylene carbon from the DEPT NMR spectrum, resonated at δ_C 22.6 (C-8″) in the ^{13}C NMR spectrum of **2** and showed a cross-peak with H-8″ in the HSQC spectrum, while the carbonyl carbon (δ_C 194.7) of compound **1** was absent in compound **2**. Thus, it was inferred that the carbonyl group of compound **1** is replaced by a methylene group in compound **2**. In addition, the HMBC correlation of the proton at δ_H 7.01 (1H, s, H-14″) to C-2″ (δ_C 149.3) allowed the establishment of the connectivity of C-9″ (δ_C 108.1) to C-2″, supporting the presence of a 2-arylbenzofuran skeleton. In turn, the HMBC correlations of H-6′ (δ_H 6.67) to C-3 (δ_C 121.4) and H-4 (δ_H 7.56) to C-1′ (δ_C 113.7) confirmed the presence of a 3-phenylcoumarin skeleton. These two units are linked through C-5′ and C-3″ by the methylene group (δ_H 3.71, δ_C 22.6), as established on the basis of the key HMBC correlations of H-8″ (δ_H 3.71) to C-4′ (δ_C 155.5), C-6′ (δ_C 131.4), C-2″ (δ_C 149.3), and C-3″a (δ_C 121.9) (Figure 2). H-6′ and H-14″ in compound **2** showed upfield shifts of 0.85 and 0.31 ppm, respectively, compared with compound **1**, in which H-6′ and H-14″ are each at a position β to a double bond conjugated with an electron-withdrawing group, the carbonyl group (C-8″). The absence of this carbonyl group at C-8″ in compound **2** resulted in the lack of inductive deshielding effects on the β-protons. In addition, the spatial arrangement of H-6′ relative to the carbonyl group (C-8″) in compound **1** may also contribute to the anisotropic deshielding effect on H-6′, while there is no such effect in compound **2** since this carbonyl group at C-8″ is absent. All of the other protons and carbons of compound **2** were assigned on the basis of the comparison of the NMR data of compounds **1** and **2**, and the assignments were confirmed by the detailed analysis of their HMBC correlations (Table S1 and Figure S2 in the Supporting Information). In the ESIMS/MS spectrum of **2**, the molecular ion peak at m/z 683.24 $[M + Na]^+$ was dissociated between the methylene group and the 2-arylbenzofuran skeleton through a quinone methide fragmentation[9,10] to give two fragments at m/z 373.14 $[M + Na - C_{19}H_{18}O_4]^+$ and m/z 333.14 $[M + Na - C_{21}H_{18}O_5]^+$, accounting for the most abundant daughter ions (Figure 3 and Figure S13m in the Supporting Information). This fragmentation pathway is similar to that previously reported for some hydroxyphenylflavanones, in which the fragmentation occurred between the methylene group and the flavanone skeleton.[11] Hence, the structure of **2** was established unambiguously as shown in Figure 1. This compound (sphenostylisin B) has a novel carbon skeleton different from that of compound **1**, with a 3-phenylcoumarin moiety coupled with a 2-arylbenzofuran unit through a methylene group.

The molecular formula of sphenostylisin C (**3**) was assigned as $C_{40}H_{38}O_9$ on the basis of the $[M + Na]^+$ ion peak at m/z 685.2404 (calcd 685.2414), indicating two degrees of unsaturation less than in compound **1**. Analysis of the 1D and 2D NMR spectra of **3** (Table S1 and Figure S3 in the Supporting Information), which were closely comparable to those of compound **1**, revealed that **3** also comprises two fragments (A and B), each including a 15-carbon skeleton with an α,α-dimethylallyl side chain. The ^1H NMR spectrum of fragment A (Table 1) clearly indicated the presence of an ABMXY spin system in the heterocyclic region [δ_H 4.09 (1H, br d, J = 9.7 Hz, H-2β), 3.77 (1H, t, J = 9.7 Hz, H-2α), 3.25 (1H, m, H-3), 2.87 (1H, dd, J = 15.1, 11.7 Hz, H-4α), and 2.64 (1H, dd, J = 15.1, 3.5 Hz, H-4β)], characteristic of the spin pattern of an isoflavan heterocycle.[12,13] This assignment was supported by the H-2α/H-2β, H-2α/H-3, H-2β/H-3, H-3/H-4α, H-3/H-4β, and H-4α/H-4β $^1H-^1H$ COSY correlations along with the HMBC correlations of H-2α and H-2β to C-3 (δ_C 31.4), C-4 (δ_C 29.7), C-8a (δ_C 152.6), and C-1′ (δ_C 118.6); of H-3 to C-1′ (δ_C 118.6), C-2′ (δ_C 157.8), and C-6′ (δ_C 128.1); and of H-4α and H-4β to C-2 (δ_C 69.2), C-5 (δ_C 127.7), C-8a (δ_C 152.6), and C-1′ (δ_C 118.6) (Figure 2). Compared with compound **1**, the replacement of the 3-phenylcoumarin skeleton by a similar isoflavan skeleton in compound **3** resulted in the lack of an α,β-unsaturated ketone functional group, thus accounting for the two fewer degrees of unsaturation and leading to the upfield shifts of H-5 (δ_H 6.81), H-8 (δ_H 6.24), and H-6′ (δ_H 7.23). These proton signals were assigned from the HMBC correlations of H-5 to C-4 (δ_C 29.7), C-7 (δ_C 154.5), and C-8a (δ_C 152.6); of H-8 to C-4a (δ_C 111.6) and C-6 (δ_C 126.1); and of H-6′ to C-3 (δ_C 31.4), C-2′ (δ_C 157.8), and C-4′ (δ_C 154.7). The structure of fragment B of compound **3** was elucidated as being the same as that in compound **1** on the basis of the comparison of their ^1H and ^{13}C NMR data, and this was confirmed from the DEPT, $^1H-^1H$ COSY, HSQC, and HMBC data (Table S1 and Figure S3 in the Supporting Information). According to the key HMBC correlation between H-6′ and C-2″ (Figure 2 and

dx.doi.org/10.1021/jo401573h | J. Org. Chem. 2013, 78, 10166−10177

Figure S3g in the Supporting Information), the connectivity between fragments A and B of compound **3** was established as being the same as that of compound **1**. In the tandem mass spectrum of **3**, both the protonated and sodiated molecular ion peaks before fragmentation were observed at *m*/*z* 663.22 $[M + H]^+$ and 685.21 $[M + Na]^+$, respectively. The protonated molecular ion peak at *m*/*z* 663.22 $[M + H]^+$ was fragmented in a more facile manner under the dissociation conditions used and thus was isolated for MS/MS fragmentation. A fragment peak at *m*/*z* 645.21 $[M + H - H_2O]^+$ was observed (Figure S13n in the Supporting Information), which was produced through loss of one water molecule from the parent ion via the same fragmentation mechanism as in compound **1**. Besides this fragment, two predominant daughter ions occurred at *m*/*z* 429.05 $[M + H - H_2O - C_{14}H_{16}O_2]^+$ and *m*/*z* 485.13 $[M + H - H_2O - C_{11}H_{12}O]^+$, resulting from heterocyclic ring fissions of the isoflavan skeleton.[9,14,15] In addition, another fragment arising through retro-Diels–Alder fragmentation was observed at *m*/*z* 191.08 $[M + H - H_2O - C_{28}H_{22}O_6]^+$ (Figure S14 in the Supporting Information). Thus, the full planar structure of **3** was assigned as shown.

The absolute configuration at C-3 of compound **3** was determined by electronic circular dichroism (ECD) analysis. In addition to the absolute configuration at C-3, the position of the conformational equilibrium of the dihydropyran ring also markedly influences the optical activity of isoflavans,[16] so an analysis of the conformation that the dihydropyran ring may adopt was performed before ECD measurement. The favored conformation of the dihydropyran ring of the isoflavan skeleton is proposed to be the half-chair on the basis of the minimization of torsional strain as established previously.[12,16,17] This results in four possible conformers: the (3*S*)-*eq* conformer, the (3*S*)-*ax* conformer, the (3*R*)-*eq* conformer, and the (3*R*)-*ax* conformer. The coupling pattern of the dihydropyran ring observed in the ^{1}H NMR spectrum of **3** showed that H-3 exhibited much larger coupling constants with H-2*ax* (J = 9.7 Hz) and H-4*ax* (J = 11.7 Hz) relative to those with H-2*eq* (J too small to be observed) and H-4*eq* (J = 3.5 Hz) (Figure S3b in the Supporting Information). This indicated that H-3 is in an axial orientation while the larger 3-phenyl substituent is equatorial (Figure 4). This deduction was consistent with the coupling patterns and constants previously reported for isoflavans with the 3-phenyl group oriented at the equatorial position[12,17] and was also supported by the H-2*eq*/H-3, H-2*ax*/H-4*ax*, and H-3/H-4*eq* NOESY correlations (Figure 4 and Figure S3i in the Supporting Information). The *S* absolute configuration at C-3 was proposed on the basis of the ECD spectrum, which demonstrated a positive Cotton effect in the ^1L_a transition region (230–250 nm) and a negative Cotton effect in the ^1L_b region (276–300 nm), as shown in Figure S15 in the Supporting Information; these results are comparable to the reported ECD data of a structurally similar 3*S* isoflavan–isoflavone dimer[12] and other (3*S*)-*eq* isoflavan conformers with oxygenation on both the A and B rings.[16,18] Therefore, the full structure of sphenostylisin C (**3**) was established. This compound shares the same novel carbon skeleton as compound **1**.

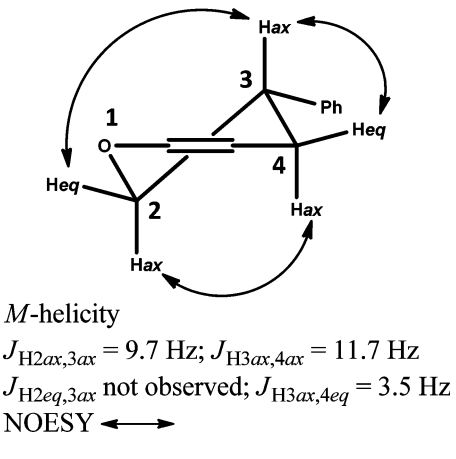

Figure 4. (3*S*)-*eq* half-chair conformer of the dihydropyran ring of compound **3**, showing the observed proton coupling constants and key NOESY correlations.

The HRESIMS spectrum of sphenostylisin D (**4**) exhibited a sodiated molecular ion peak at *m*/*z* 361.1046 (calcd 361.1052), consistent with a molecular formula of $C_{20}H_{18}O_5$. The UV spectrum of **4** was typical of a 3-phenylcoumarin skeleton.[6] The ^{1}H NMR spectrum of **4** showed a singlet at δ_H 7.80 (1H, H-4) (Table 2), indicating it to be a characteristic proton located at C-4 in a 3-phenylcoumarin skeleton. The remaining signals observed in the ^{1}H NMR spectrum showed the presence of a 1,2,4-trisubstituted benzene ring [δ_H 7.03 (1H, d, J = 8.3 Hz, H-6′), 6.35 (1H, d, J = 2.2 Hz, H-3′), and 6.26 (1H, dd, J = 8.3, 2.2 Hz, H-5′)], a 1,3,4,6-tetrasubstituted benzene ring [δ_H 7.45 (1H, s, H-5) and 6.74 (1H, s, H-8)], and an α,α-dimethylallyl group [δ_H 6.23 (1H, dd, J = 17.5, 10.7 Hz, H-10), 4.95 (1H, dd, J = 10.7, 1.2 Hz, H-11a), 4.93 (1H, dd, J = 17.5, 1.2 Hz, H-11b), and 1.45 (6H, s, CH_3 × 2, H-12/13)]. The ^{13}C NMR spectrum of **4** showed 20 carbon signals, which were classified as two methyls, five quaternary carbons, seven tertiary sp^2 carbons, one secondary sp^2 carbon, four oxygen-bearing tertiary sp^2 carbons, and a lactone carbonyl group on the basis of the DEPT and HSQC data. The characteristic NMR data of **4** were found to be very similar to those of fragment A of compound **1**, while the absence of any fragment B resulted in an additional proton signal (H-5′) as well as an upfield shift of 0.49 ppm for H-6′ in compound **4**. The H-3′, H-5′, and H-6′ resonances of the trisubstituted aromatic ring were assigned on the basis of the coupling constants and the ^{1}H–^{1}H COSY spectrum, and the assignments were corroborated by the HMBC correlations of H-3′ to C-1′ (δ_C 113.8), C-2′ (δ_C 156.0), and C-5′ (δ_C 106.2); of H-5′ to C-1′ (δ_C 113.8), C-3′ (δ_C 102.6), and C-6′ (δ_C 131.5); and of H-6′ to C-2′ (δ_C 156.0) and C-4′ (δ_C 158.3). In addition, the HMBC cross-peak between H-6′ and C-3 (δ_C 121.0) confirmed that this trisubstituted benzene ring is linked at C-3. The assignments of the two singlets at δ_H 7.45 (H-5) and 6.74 (H-8) were based on the HMBC correlations of H-5 to C-4 (δ_C 142.1), C-7 (δ_C 159.1), and C-8a (δ_C 153.0) and of H-8 to C-4a (δ_C 111.2) and C-6 (δ_C 131.6). The linkage of the α,α-dimethylallyl group at C-6 (δ_C 131.6) was established by the observed HMBC correlations of H-10, H-12, and H-13 to C-6 and confirmed by the HMBC correlation of H-5 to C-9 (δ_C 39.9). Thus, sphenostylisin D (**4**) was assigned as 7-hydroxy-6-(2-methylbut-3-en-2-yl)-2′,4′-dihydroxy-3-phenylcoumarin.

Sphenostylisins E–G (**5**–**7**) were found to share the same molecular formula, $C_{20}H_{18}O_6$, on the basis of analysis of their HRESIMS data, which showed $[M + Na]^+$ ion peaks at *m*/*z* 377.1007, 377.0991, and 377.0993, respectively (calcd 377.1001). When compared with compound **4**, this molecular formula indicated that compounds **5**–**7** have the same degree of unsaturation with one more oxygen present, implying that a

dx.doi.org/10.1021/jo401573h | J. Org. Chem. 2013, 78, 10166–10177

Table 2. ^{1}H and ^{13}C NMR Spectroscopic Data of Compounds 4−8[a]

	4		5		6		7		8	
no.	δ_H[b]	δ_C[c]	δ_H[b]	δ_C[c]	δ_H[b]	δ_C[c]	δ_H[b]	δ_C[c]	δ_H[b]	δ_C[c]
2		160.3		163.7		164.0		160.3	8.10, s	156.3
3		121.0		122.9		122.9		120.9		124.1
4	7.80, s	142.1	7.87, s	144.2	7.79, s	144.1	7.80, s	142.2		179.2
4a		111.2		115.3		113.7		111.3		117.0
5	7.45, s	126.4	7.38, s	122.6	7.33, s	132.7	7.45, s	128.3	8.13, s	127.4
6		131.6		137.2		124.4		129.1		133.3
7		159.1		162.8		161.4		159.2		164.1
8	6.74, s	102.3	6.76, s	98.4	6.75, s	103.4	6.72, s	102.3	6.86, s	104.0
8a		153.0		156.0		155.2		153.0		158.5
9		39.9		43.7		75.3		46.1		48.0
10	6.23, dd (17.5, 10.7)	147.1	4.45, dd (6.3, 5.3)	95.6	6.01, dd (17.3, 10.8)	146.0	6.26, dd (17.6, 10.8)	144.1	6.33, dd (17.4, 10.6)	144.6
11a	4.95, dd (10.7, 1.2)	110.5	3.86, br d (5.3)	61.9	5.20, dd (17.3, 1.2)	112.2	5.02, dd (10.8, 1.1)	112.5	5.14, br d (10.6)	113.8
11b	4.93, dd (17.5, 1.2)		3.85, br d (6.3)		5.00, dd (10.8, 1.2)		4.92, dd (17.6, 1.1)		5.04, br d (17.4)	
12a	1.45, s	26.9	1.44, s	28.2	2.92, d (13.9)	43.6	3.79, d (10.3)	67.1	4.03, d (10.7)	69.3
12b					2.87, d (13.9)		3.72, d (10.3)		3.89, d (10.7)	
13	1.45, s	26.9	1.25, s	23.2	1.26, s	27.0	1.41, s	21.8	1.53, s	22.4
1′		113.8		115.4		115.6		113.7		112.3
2′		156.0		157.4		157.4		156.0		158.0
3′	6.35, d (2.2)	102.6	6.38, d (2.3)	104.0	6.38, d (2.3)	104.0	6.35, d (2.2)	102.6	6.40, d (2.2)	104.7
4′		158.3		160.0		160.0		158.3		160.2
5′	6.26, dd (8.3, 2.2)	106.2	6.35, dd (8.2, 2.3)	107.9	6.35, dd (8.2, 2.3)	107.9	6.25, dd (8.3, 2.2)	106.2	6.38, dd (8.2, 2.2)	108.3
6′	7.03, d (8.3)	131.5	7.12, d (8.2)	132.7	7.11, d (8.2)	132.7	7.02, d (8.3)	131.5	7.05, d (8.2)	132.9

[a]NMR data obtained in DMSO-d_6 for **4** and **7** and in CD_3OD for **5**, **6**, and **8**. Assignments are based on $^{1}H-^{1}H$ COSY, HSQC, and HMBC spectroscopic data. [b]Measured at 400 MHz for ^{1}H NMR; presented as δ in ppm, multiplicity (J in Hz). [c]Measured at 100 MHz for ^{13}C NMR; δ in ppm.

carbon in **4** has been oxygenated to give compounds **5**−**7**. The NMR spectroscopic data of **5**−**7** (Table 2 and Figures S5−S7 in the Supporting Information) were closely comparable to those of **4**, with the only differences evident in signals for the side chain at C-6. Thus, an α,α-dimethylallyl group at C-6 in **4** was replaced by a 3-methylbutane-1,2-diol moiety in **5**. The signals of the latter unit occurred at δ_H 4.45 (1H, dd, J = 6.3, 5.3 Hz, H-10), 3.86 (1H, br d, J = 5.3 Hz, H-11a), 3.85 (1H, br d, J = 6.3 Hz, H-11b), 1.44 (3H, s, H-12), and 1.25 (3H, s, H-13) in the ^{1}H NMR spectrum as well as at δ_C 43.7 (C, C-9), 95.6 (CH, C-10), 61.9 (CH_2, C-11), 28.2 (CH_3, C-12), and 23.2 (CH_3, C-13) in the ^{13}C NMR spectrum. In addition, key HMBC correlations of H-10 to C-9, C-11, C-12 and C-13 as well as H-11, H-12, and H-13 to C-9 and C-10 supported the structure assigned for the side-chain moiety in **5**. Moreover, this side chain formed a dihydrofuran ring with C-6 (δ_C 137.2) and C-7 (δ_C 162.8), as suggested by the HMBC correlations of H-10 to C-6 and C-7 and of H-12 and H-13 to C-6. Thus, the structure of sphenostylisin E (**5**) was established as 6-(2,7-epoxy-3-methylbut-1-ol-3-yl)-2′,4′-dihydroxy-3-phenylcoumarin.

Compound **6** showed side-chain signals at δ_H 6.01 (1H, dd, J = 17.3, 10.8 Hz, H-10), 5.20 (1H, dd, J = 17.3, 1.2 Hz, H-11a), 5.00 (1H, dd, J = 10.8, 1.2 Hz, H-11b), 2.92 (1H, d, J = 13.9 Hz, H-12a), 2.87 (1H, d, J = 13.9 Hz, H-12b), and 1.26 (3H, s, H-13) in the ^{1}H NMR spectrum along with corresponding ^{13}C NMR data at δ_C 75.3 (C, C-9), 146.0 (CH, C-10), 112.2 (CH_2, C-11), 43.6 (CH_2, C-12), and 27.0 (CH_3, C-13) (Table 2). The downfield shift of C-9 to δ_C 75.3 suggested that C-9 is oxygenated. These signals together indicated a 2-methylbut-3-en-2-ol side chain in **6** when compared with those of **4**. This side chain was connected to C-6 (δ_C 124.4), as determined by the long-range correlations of H-12 to C-5 (δ_C 132.7) and C-7 (δ_C 161.4) and of H-5 (δ_H 7.33) to C-12 (δ_C 43.6) in the HMBC spectrum. Therefore, the structure of sphenostylisin F (**6**) was determined to be 7-hydroxy-6-(2-hydroxy-2-methylbut-3-en-1-yl)-2′,4′-dihydroxy-3-phenylcoumarin.

Comparison of the NMR data in Table 2 showed that one of the geminal dimethyl groups of the side chain in **4** was replaced by a hydroxymethyl group (δ_H 3.79, 3.72; δ_C 67.1) in **7**, which was the only apparent difference between these two compounds. The ^{1}H NMR signals at δ_H 6.26 (1H, dd, J = 17.6, 10.8 Hz, H-10), 5.02 (1H, dd, J = 10.8, 1.1 Hz, H-11a), 4.92 (1H, dd, J = 17.6, 1.1 Hz, H-11b), 3.79 (1H, d, J = 10.3 Hz, H-12a), 3.72 (1H, d, J = 10.3 Hz, H-12b), and 1.41 (3H, s, H-13) and the ^{13}C NMR signals at δ_C 46.1 (C, C-9), 144.1 (CH, C-10), 112.5 (CH_2, C-11), 67.1 (CH_2, C-12), and 21.8 (CH_3, C-13) were assigned to the side chain in **7**, a 1-hydroxymethyl-1-methylallyl group. The linkage of this side chain at C-6 (δ_C 129.1) was confirmed by the HMBC correlations of H-10, H-12, and H-13 to C-6 and of H-5 (δ_H 7.45) to C-9. Hence, sphenostylisin G (**7**) was established structurally as 7-hydroxy-6-(1-hydroxy-2-methylbut-3-en-2-yl)-2′,4′-dihydroxy-3-phenylcoumarin.

Compounds **5**−**7** are isomers with different arrangements only in their respective side chain at C-6. These side chains are considered to be derived from an α,α-dimethylallyl group through oxidation, rearrangement, and cyclization (Scheme S1 in the Supporting Information). To the best of our knowledge, this is the first report of the presence of these side chains among the naturally occurring 3-phenylcoumarins.

dx.doi.org/10.1021/jo401573h | J. Org. Chem. 2013, 78, 10166−10177

Table 3. ^{1}H and ^{13}C NMR Spectroscopic Data of Compounds 9−11[a]

	9		10		11	
no.	δ_H[b]	δ_C[c]	δ_H[b]	δ_C[c]	δ_H[b]	δ_C[c]
1		112.3		112.2		112.2
2		164.4		164.5		164.5
3	6.24, d (2.3)	102.4	6.23, d (2.3)	102.4	6.19, d (2.3)	102.4
4		164.7		164.6		164.8
5	6.38, dd (8.8, 2.3)	108.0	6.34, dd (8.9, 2.3)	108.0	6.32, dd (8.9, 2.3)	108.1
6	7.94, d (8.8)	133.1	7.89, d (8.9)	133.2	7.91, d (8.9)	133.2
7		202.9		203.2		203.1
8a	4.11, d (16.3)	38.7	4.01, d (15.7)	38.4	3.99, br s	38.5
8b	4.03, d (16.3)		3.96, d (15.7)			
1′		113.4		111.9		111.3
2′		154.8		153.9		153.9
3′	6.23, s	96.8	6.30, s	102.7	6.29, s	103.5
4′		157.5		155.2		155.2
5′		127.6		114.9		121.6
6′	6.83, s	124.2	6.73, s	134.2	6.83, s	130.5
7′		42.1	2.57, s	42.1		45.6
8′	4.16, dd (6.7, 5.2)	92.8		73.5	6.20, dd (17.6, 10.6)	145.0
9′a	3.65, m	60.0	5.89, dd (17.3, 10.7)	146.0	4.96, br d (10.6)	111.7
9′b					4.89, br d (17.6)	
10′a	1.27, s	27.2	5.08, dd (17.3, 1.9)	110.7	3.67, d (10.5)	67.6
10′b			4.87, dd (10.7, 1.9)		3.65, d (10.5)	
11′	1.02, s	23.2	1.07, s	26.4	1.29, s	21.4

[a]NMR data obtained in DMSO-d_6 for **9**−**11**. Assignments are based on ^{1}H−^{1}H COSY, HSQC, and HMBC spectroscopic data. [b]Measured at 400 MHz for ^{1}H NMR; presented as δ in ppm, multiplicity (J in Hz). [c]Measured at 100 MHz for ^{13}C NMR; δ in ppm.

The molecular formula of sphenostylisin H (**8**) was determined to be $C_{20}H_{18}O_6$ from the molecular ion peak $[M + Na]^+$ at m/z 377.0995 (calcd 377.1001) in the HRESIMS spectrum, the same as those of compounds **5**−**7**. However, the diagnostic H-2 vinylic singlet at δ_H 8.10 (H-2) in the ^{1}H NMR spectrum of **8** indicated the presence of an isoflavone skeleton instead of a coumarin skeleton. The B-ring protons displayed an ABX spin system in the ^{1}H NMR spectrum at δ_H 7.05 (1H, d, J = 8.2 Hz, H-6′), 6.40 (1H, d, J = 2.2 Hz, H-3′), and 6.38 (1H, dd, J = 8.2, 2.2 Hz, H-5′). These chemical shifts suggested that the B-ring is a 2′,4′-dihydroxybenzene unit rather than a 3′,4′-dihydroxybenzene moiety according to the literature,[19] which was confirmed by the HMBC spectrum, in which only H-6′ showed an HMBC correlation to C-3 (δ_C 124.1). The aromatic region of the ^{1}H NMR spectrum also exhibited two one-proton singlets at δ_H 8.13 and 6.86, which were assigned to H-5 and H-8 of the isoflavone A-ring, respectively, on the basis of the HMBC correlations of H-5 to C-4 (δ_C 179.2) and C-8a (δ_C 158.5) and of H-8 to C-4a (δ_C 117.0). In addition, the ^{1}H NMR signals at δ_H 6.33 (1H, dd, J = 17.4, 10.6 Hz, H-10), 5.14 (1H, br d, J = 10.6 Hz, H-11a), 5.04 (1H, br d, J = 17.4 Hz, H-11b), 4.03 (1H, d, J = 10.7 Hz, H-12a), 3.89 (1H, d, J = 10.7 Hz, H-12b), and 1.53 (3H, s, H-13) along with the ^{13}C NMR signals at δ_C 48.0 (C, C-9), 144.6 (CH, C-10), 113.8 (CH_2, C-11), 69.3 (CH_2, C-12), and 22.4 (CH_3, C-13) (Table 2) were characteristic of a 1-hydroxymethyl-1-methylallyl side chain, the same as in **7**. Moreover, H-10, H-12, and H-13 are correlated to C-6 (δ_C 133.3) and H-5 (δ_H 8.13) is correlated to C-9 in the HMBC spectrum, establishing the connectivity of this side chain to C-6. Accordingly, sphenostylisin H (**8**) was established structurally as 7-hydroxy-6-(1-hydroxy-2-methylbut-3-en-2-yl)-2′,4′-dihydroxyisoflavone.

The molecular formula of sphenostylisin I (**9**), $C_{19}H_{20}O_6$, was determined by HRESIMS, which gave an $[M + Na]^+$ ion peak at m/z 367.1151 (calcd 367.1158). The characteristic UV spectrum and the typical ^{1}H NMR signals at δ_H 4.11 (1H, d, J = 16.3 Hz, H-8a) and 4.03 (1H, d, J = 16.3 Hz, H-8b) combined with the corresponding ^{13}C NMR signals at δ_C 202.9 (C-7) and 38.7 (C-8) (Table 3) revealed that **9** has a deoxybenzoin skeleton.[20,21] Additional ^{1}H NMR signals observed for this skeleton included an ABX aromatic spin system [δ_H 7.94 (1H, d, J = 8.8 Hz, H-6), 6.38 (1H, dd, J = 8.8, 2.3 Hz, H-5), and 6.24 (1H, d, J = 2.3 Hz, H-3)] and two aromatic protons at *para* positions [δ_H 6.83 (1H, s, H-6′) and 6.23 (1H, s, H-3′)], while the corresponding ^{13}C NMR signals observed were three quaternary carbons [δ_C 112.3 (C-1), 113.4 (C-1′), and 127.6 (C-5′)], five tertiary sp^2 carbons [δ_C 102.4 (C-3), 108.0 (C-5), 133.1 (C-6), 96.8 (C-3′), and 124.2 (C-6′)], and four oxygen-bearing tertiary sp^2 carbons [δ_C 164.4 (C-2), 164.7 (C-4), 154.8 (C-2′), and 157.5 (C-4′)]. These NMR data were very similar to those of maackiaphenone, a known deoxybenzoin compound isolated from *Maackia tenuifolia*,[21] with the only evident difference being in the side chain. The side-chain resonances of **9** occurred at δ_H 4.16 (1H, dd, J = 6.7, 5.2 Hz, H-8′), 3.65 (2H, m, H-9′), 1.27 (3H, s, H-10′), and 1.02 (3H, s, H-11′) as well as at δ_C 42.1 (C, C-7′), 92.8 (CH, C-8′), 60.0 (CH_2, C-9′), 27.2 (CH_3, C-10′), and 23.2 (CH_3, C-11′), consistent with a 3-methylbutane-1,2-diol moiety fused with C-4′ and C-5′ to form a dihydrofuran ring, the same as in **5**, and this was confirmed by HMBC correlations (Table S3 and Figure S9 in the Supporting Information). Thus, the structure of sphenostylisin I (**9**) was determined to be 2,4-dihydroxy-2′-dihydroxy-5′-(2,4′-epoxy-3-methylbut-1-ol-3-yl)deoxybenzoin.

Sphenostylisin J (**10**) and sphenostylisin K (**11**) gave the same molecular formula as for **9**, $C_{19}H_{20}O_6$, on the basis of their HRESIMS data. Comparison of their 1D and 2D NMR spectra with those of **9** revealed the presence of the same skeleton in both **10** and **11**, with the only difference being due

dx.doi.org/10.1021/jo401573h | J. Org. Chem. 2013, 78, 10166−10177

Scheme 1. Cyclization Reaction of 9 To Form a 2-Arylbenzofuran Skeleton

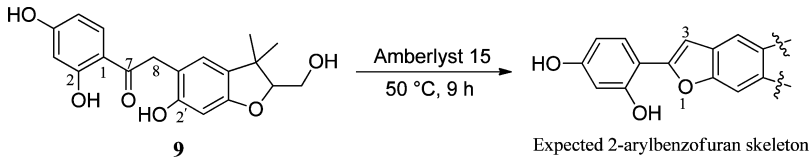

9 Expected 2-arylbenzofuran skeleton

Table 4. Hydroxyl Radical-Scavenging, Quinone Reductase-Inducing, NF-κB Inhibitory, and Cytotoxic Activities of Compounds 1−11

	hydroxyl radical-scavenging	quinone reductase induction			NF-κB inhibition	cytotoxicity
compound	ED_{50} (μM)[a]	CD (μM)[b]	IC_{50} (μM)[c]	CI[d]	IC_{50} (μM)[e]	IC_{50} (μM)[f]
1	0.71	7.4	9.2	1.3	0.006	1.6
2	0.73	3.0	10.8	3.6	1.5	4.5
3	0.94	2.1	15.6	7.4	0.44	4.2
4	2.6	13.3	41.3	3.1	0.06	>10
5	18.5	>20	>100	NA[g]	0.70	>10
6	>20	>20	>100	NA[g]	0.34	>10
7	>20	>20	>100	NA[g]	0.23	>10
8	2.2	13.0	>100	>7.7	0.45	>10
9	1.0	19.6	74.3	3.8	>20	>10
10	0.60	>20	>100	NA[g]	>20	>10
11	0.63	>20	>100	NA[g]	>20	>10
quercetin[h]	1.2					
L-sulforaphane[i]		0.71	15.2	21.4		
rocaglamide[j]					0.08	
paclitaxel[k]						0.0006

[a]Concentration scavenging hydroxyl radical by 50%. Compounds with ED_{50} values of <20 μM are considered active. [b]Concentration required to double the quinone reductase activity. Compounds with CD values of <20 μM are considered active. [c]Concentration inhibiting hepa-1c1c7 cell growth by 50%. [d]Chemoprevention index (equal to IC_{50}/CD). [e]Concentration inhibiting NF-κB p65 by 50%. Compounds with IC_{50} values of <20 μM are considered active. [f]Concentration inhibiting HT-29 cell growth by 50%. Compounds with IC_{50} values of <10 μM are considered active. [g]NA = not applicable. [h]Positive control for the hydroxyl radical-scavenging assay. [i]Positive control for the quinone reductase induction assay. [j]Positive control for the NF-κB p65 inhibition assay. [k]Positive control for the cytotoxicity assay against the HT-29 cell line.

to rearrangements of the isoprenyl side chain at C-5′. Compound **10** has a 2-methylbut-3-en-2-ol side chain as in **6**, while compound **11** has a 1-hydroxymethyl-1-methylallyl substituent as in **7** and **8**. Hence, the structures of **10** and **11** were established as 2,4-dihydroxy-2′,4′-dihydroxy-5′-(2-hydroxy-2-methylbut-3-en-1-yl)deoxybenzoin and 2,4-dihydroxy-2′,4′-dihydroxy-5′-(1-hydroxy-2-methylbut-3-en-2-yl)-deoxybenzoin, respectively, by comparison of their NMR data with those of **9** and confirmed by detailed 2D NMR spectroscopic data analysis (Table S3 and Figures S9 and S10 in the Supporting Information). To the best of our knowledge, the side chains of **9**−**11** have not been reported to be present in other naturally occurring deoxybenzoin derivatives to date.

A plausible biogenetic pathway for the generation of sphenostylisins A−K (**1**−**11**) is proposed in Scheme S1 in the Supporting Information. From a biogenetic perspective, **1**−**11** may all be considered as isoflavonoid derivatives in a broad sense, despite their different structures. It has been validated in previous investigations that isoflavone is involved in the first step of isoflavonoid biosynthesis, with the basic skeleton being constructed for different subclasses of isoflavonoids before any isoprenoid substituents are added.[22] Accordingly, 2′-hydroxydaidzein, an isoflavone previously isolated from some Fabaceae species,[23] is proposed as a precursor. Simple prenylation and hydroxylation of this precursor could lead to the generation of compound **8**. As relatively well characterized by previous investigations, the isoflavan (fragment A of **3**) and 3-phenylcoumarin (**4**, fragment A of **1** and **2**) would be biosynthesized from isoflavone,[22] followed by prenylation and then diverse modifications of the prenyl side chains[24] to form **5**−**7**. The class of arylbenzofurans (fragment B of **1**−**3**) is proposed to be produced by 4-pyrone ring cleavage, recyclization, and then reduction.[25−27] The assembly mechanism of fragments A and B via carbon−carbon linkage in compounds **1**−**3** is believed to be comparable to that of existing bioflavonoids, although this is still a matter of conjecture. The deoxybenzoins (**9**−**11**) appear to be derived by 4-pyrone ring opening, oxidation of aldehyde to carboxylic acid, and then loss of one carbon atom through decarboxylation.[25,28] It is interesting that this class of compounds has been reported to usually co-occur with various structurally related isoflavonoids,[20−22] and their stability during isolation was considered to be due to the hydrogen bonding of the *ortho* OH-2 to the carbonyl. It has been demonstrated that the lack of an *ortho* OH-2 group results in spontaneous cyclization to give benzofuran derivatives.[25] On the basis of these observations, it was assumed in previous investigations that deoxybenzoins could be the precursors of arylbenzofurans.[20,21] Thus, in the present study, a cyclization reaction of **9** was performed via acid treatment with Amberlyst 15 resin, and the expected 2-arylbenzofuran skeleton was generated (Scheme 1), supporting the assumption mentioned above that suggests a possible link among different classes of isoflavonoid compounds and also supporting the structure elucidation of the deoxybenzoin skeleton characterized for compounds **9**−**11** in the present study.

dx.doi.org/10.1021/jo401573h | J. Org. Chem. 2013, 78, 10166−10177

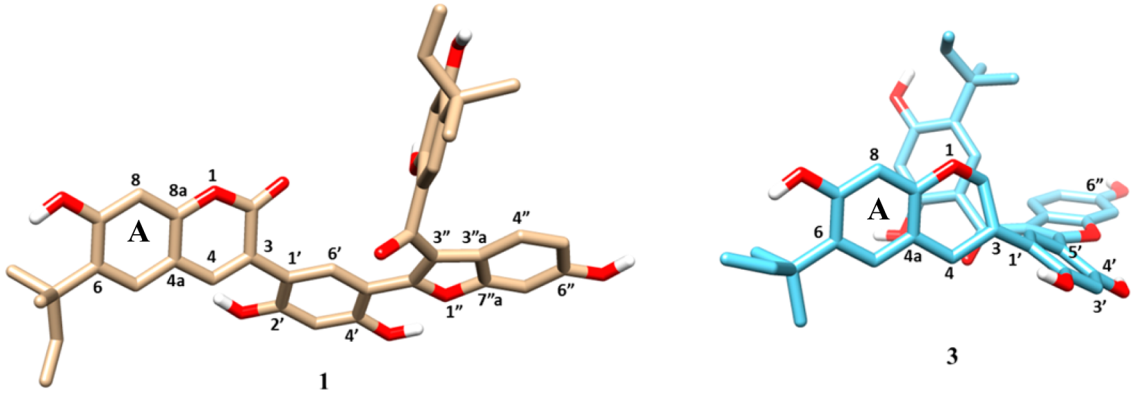

Figure 5. Conformational models of **1** and **3** produced using the LigPrep/ConfGen software suite, with the A-rings placed in the same plane.

All 11 new compounds isolated in the present investigation (**1**−**11**) were evaluated biologically. As shown in Table 4, eight compounds (**1**−**4** and **8**−**11**) exhibited potent hydroxyl radical-scavenging activity (ED_{50} values ranging from 0.60 to 2.6 μM) comparable to that of the positive control, quercetin (ED_{50} = 1.2 μM), with sphenostylisin J (**10**) (ED_{50} = 0.60 μM) being the most active. Six compounds (**1**−**4**, **8**, and **9**) exhibited QR-inducing activity, with sphenostylisin C (**3**) (CD = 2.1 μM) exhibiting the most potent effect. Eight compounds (**1**−**8**) showed NF-κB p65 inhibitory activity. In particular, sphenostylisin A (**1**), representative of a novel carbon skeleton, was found to be a very potent NF-κB p65 inhibitor that exhibited an IC_{50} value of 6 nM and was >10 times more potent than the positive control, rocaglamide. A comparison of the NF-κB p65 inhibitory activities of compounds **1**−**11** showed an interesting preliminary structure−activity relationship (SAR) among those compounds. The 3-phenylcoumarin derivatives with different side chains, **4**−**7**, exhibited similarly potent NF-κB inhibitory activities, which implies that the 3-phenylcoumarin skeleton is important in mediating this type of activity. In contrast, the deoxybenzoins **9**−**11** lacking a lactone ring lost activity, indicating that a lactone ring is also important for activity. This deduction was supported by the observation that compound **1** incorporating a 3-phenylcoumarin moiety exhibited 75-fold greater potency than compound **3**, which contains an isoflavan unit instead of a 3-phenylcoumarin unit. This striking difference between the potencies of **1** and **3** in the NF-κB inhibition assay can be rationalized through the following analysis. First, the carbonyl group (C-2) of the lactone, which is present in **1** but absent in **3**, may form hydrogen-bonding interactions with key residues in the active sites of the proteins associated with NF-κB p65 inhibition. Second, energy-minimized conformational models of **1** and **3** generated using the LigPrep/ConfGen software suite suggested that **1** bears a more extended conformation than **3** (Figure 5). The half-chair conformation of the dihydropyran ring in **3** sets the 3-phenyl ring almost perpendicular to the dihydropyran ring, while the 3-phenyl ring in **1** is comparatively closer to being planar with the lactone ring because of the presence of the double bond between C-3 and C-4. The C-3−C-4−C-1′−C-6′ dihedral angles in **1** and **3** are 138.2° and 82.9°, respectively. The distance between C-6 and C-6″ in **1** is about 1 Å longer than that in **3**. It is conjectured that bioactive small molecules favor extended conformations that intuitively expose more hydrophobic surfaces to contact with the receptor, in comparison with folded conformations.[29,30] Thus, the more extended conformation of **1** may imply more extensive interactions with protein residues. Another interesting result observed in the NF-κB p65 inhibitory activity data is that compound **4**, the 3-phenylcoumarin moiety of **1**, retains 1/10 of the activity of **1**, indicating that the 3-phenylbenzofuran moiety of **1** either facilitates the binding affinity or improves the penetration of the compound into the cell. In addition to the potent NF-κB p65 inhibitory activity, sphenostylisin A (**1**) also showed cytotoxicity against the HT-29 cell line (IC_{50} = 1.6 μM).

EXPERIMENTAL SECTION

General Experimental Procedures. Optical rotations were measured on a polarimeter. UV spectra were run on a spectrophotometer. Electronic circular dichroism (ECD) spectra were recorded on a spectropolarimeter. IR spectra were obtained on an IR spectrometer. NMR spectroscopic data were recorded at room temperature on 400, 600, and 800 MHz spectrometers. High-resolution electrospray ionization mass spectrometry (HRESIMS) was performed on a Q-Tof mass spectrometer operated in the positive-ion mode, with sodium iodide being used for mass calibration. The tandem mass spectrometric analysis was performed on an ion-trap mass spectrometer operated in the positive-ion mode. Column chromatography was performed with LH-20, silica gel, and 40−63 μm C_{18}-RP silica gel. Analytical thin-layer chromatography (TLC) was conducted on precoated 250 μm thick silica gel F_{254} glass plates. A semipreparative C_{18} column (5 μm, 150 mm × 10 mm i.d.) with a guard column (5 μm, 10 mm × 10 mm i.d.) and a preparative C_{18} column (5 μm, 150 mm × 19 mm i.d.) with a guard column (5 μm, 10 mm × 19 mm i.d.) were used for HPLC, along with a diode array detector.

Plant Material. The root bark of *S. marginata* ssp. *erecta* was collected in 1991 and recollected in 1996 at the Mazoe Hills in Zimbabwe by T.E.C., who also identified this plant. A voucher specimen (T.E. Chagwedera 187) was deposited in the National Herbarium Botanic Garden (Harare, Zimbabwe).

Extraction and Isolation. The air-dried and milled root bark (2 kg) of *S. marginata* ssp. *erecta* was extracted with methanol (3 × 8 L) at room temperature for 2 days each to afford an extract (739 g), which was suspended in H_2O (2 L) and then partitioned in turn with hexanes (3 × 2 L), $CHCl_3$ (3 × 2 L), EtOAc (3 × 2 L), and *n*-BuOH (3 × 2 L) to furnish extracts soluble in dried hexanes (21 g), $CHCl_3$ (60 g), EtOAc (30 g), *n*-BuOH (350 g), and H_2O (278 g). The $CHCl_3$-soluble extract, the most potent among these extracts in the in vitro hydroxyl radical-scavenging and QR-inducing assays, was subjected to chromatography over coarse silica gel and eluted with a CH_2Cl_2−acetone gradient (40:1, 15:1, 10:1, 8:1, 6:1, 4:1, 3:1, 2:1, 1:1, 1:2, and pure acetone) to afford 11 fractions (F01−F11). Fraction F05 (7.2 g), which was active in the hydroxyl radical-scavenging and QR-inducing assays, was chromatographed over a silica gel column with a $CHCl_3$−MeOH solvent system (30:1, 25:1, 20:1, 15:1, 12:1, 10:1, 8:1, 6:1, 5:1, 3:1, 2:1, and 1:1) to give 15 subfractions (F0501−F0515).

dx.doi.org/10.1021/jo401573h | J. Org. Chem. 2013, 78, 10166−10177

F0505 (eluted with $CHCl_3$–MeOH, 12:1; 168 mg) was further purified by HPLC using a preparative C_{18} column (5 μm, 150 mm × 19 mm i.d.) with MeOH–H_2O (65:35) at a flow rate of 8.0 mL/min to yield compound **4** (t_R = 25.5 min; 22.0 mg). F0507 (eluted with $CHCl_3$–MeOH, 10:1; 980 mg) was purified by Sephadex LH-20 column chromatography with elution by MeOH–H_2O (20:80, 40:60, 60:40, 80:20, and 100:0) to afford a further subfraction, F050703. This subfraction (357 mg) was then purified using the same HPLC column with MeOH–H_2O (48:52, flow rate 8.0 mL/min) to yield compounds **5** (t_R = 22.2 min; 5.0 mg), **6** (t_R = 35.8 min; 23.4 mg), **8** (t_R = 30.6 min; 3.0 mg), **9** (t_R = 43.4 min; 5.6 mg), and **10** (t_R = 49.1 min; 6.4 mg). F0508 (eluted with $CHCl_3$–MeOH, 8:1; 485 mg) was chromatographed initially over an LH-20 column with elution by MeOH–H_2O gradient mixtures (0:100, 25:75, 50:50, 75:25, and 100:0) to afford five subfractions (F050801–F050805). F050803 (42 mg) was then purified by HPLC on a semipreparative C_{18} column (5 μm, 150 mm × 10 mm i.d.) with isocratic elution (21% CH_3CN–79% H_2O, flow rate 4.0 mL/min) to yield compounds **7** (t_R = 35.0 min; 5.3 mg) and **11** (t_R = 46.8 min; 1.7 mg). F0512 (eluted with $CHCl_3$–MeOH, 5:1; 1.2 g) was subjected to passage over an LH-20 column using MeOH–H_2O mixtures (0:100, 20:80, 40:60, 60:40, 80:20, and 100:0) as eluting solvents to afford eight subfractions (F051201–F051208). F051204 (176 mg) was then purified using the same HPLC semipreparative C_{18} column with isocratic elution (43% CH_3CN–57% H_2O containing 0.05% TFA in H_2O) at a flow rate of 4.0 mL/min to yield compounds **1** (t_R = 37.6 min; 3.4 mg) and **3** (t_R = 46.9 min; 4.7 mg) and a further subfraction, F05120403. This subfraction (69 mg) was purified again using the same HPLC C_{18} column, eluted with MeOH–H_2O (62:38, flow rate 4.0 mL/min), to yield compound **2** (t_R = 45.0 min; 6.8 mg).

*Sphenostylisin A (**1**).* Yellow amorphous solid; UV (MeOH) λ_{max}/nm (log[ε/M^{-1} cm^{-1}]) 216 (4.60), 253 (4.32), 308 (4.38), 343 (4.39); IR (film) ν_{max} 3252, 2964, 2923, 1693, 1615, 1571, 1492, 1387, 1275, 1191 1118, 1064, 908, 841 cm^{-1}; ^1H and ^{13}C NMR data are shown in Table 1; HRESIMS obsd *m*/*z* 697.2035 $[M + Na]^+$ (calcd for $C_{40}H_{34}O_{10}Na$, 697.2050).

*Sphenostylisin B (**2**).* Yellow amorphous solid; UV (MeOH) λ_{max}/nm (log[ε/M^{-1} cm^{-1}]) 218 (4.58), 258 (4.15), 318 (4.25), 340 (4.19); IR (film) ν_{max} 3286, 2966, 2926, 1686, 1617, 1577, 1491, 1442, 1364, 1293, 1191, 1149, 1121, 1022, 842 cm^{-1}; ^1H and ^{13}C NMR data are shown in Table 1; HRESIMS obsd *m*/*z* 683.2269 $[M + Na]^+$ (calcd for $C_{40}H_{36}O_9Na$, 683.2257).

*Sphenostylisin C (**3**).* Yellow amorphous solid; $[\alpha]_D^{20}$ +23 (*c* 0.18, MeOH); UV (MeOH) λ_{max}/nm (log[ε/M^{-1} cm^{-1}]) 210 (4.87), 271 (4.37), 294 (4.42), 309 (4.39), 342 (sh, 4.12); ECD (MeOH) λ_{max}/nm ([θ]) 212 (+41693), 240 (+4312), 268 (+6305), 289 (−4626), 315 (+5501); IR (film) ν_{max} 3419, 2967, 2930, 1622, 1587, 1494, 1392, 1273, 1143, 1118, 1082, 900, 838 cm^{-1}; ^1H and ^{13}C NMR data are shown in Table 1; HRESIMS obsd *m*/*z* 685.2404 $[M + Na]^+$ (calcd for $C_{40}H_{38}O_9Na$, 685.2414).

*Sphenostylisin D (**4**).* Yellow amorphous solid; UV (MeOH) λ_{max}/nm (log[ε/M^{-1} cm^{-1}]) 206 (4.69), 248 (3.92), 350 (4.20); IR (film) ν_{max} 3308, 2968, 1683, 1615, 1575, 1508, 1423, 1366, 1285, 1188, 1166, 1102, 980, 846, 550 cm^{-1}; ^1H and ^{13}C NMR data are shown in Table 2; HRESIMS obsd *m*/*z* 361.1046 $[M + Na]^+$ (calcd for $C_{20}H_{18}O_5Na$, 361.1052).

*Sphenostylisin E (**5**).* Yellow amorphous solid; $[\alpha]_D^{20}$ +13 (*c* 0.1, MeOH); UV (MeOH) λ_{max}/nm (log[ε/M^{-1} cm^{-1}]) 206 (4.64), 248 (3.86), 350 (4.14); IR (film) ν_{max} 3319, 2961, 2926, 1699, 1621, 1576, 1482, 1390, 1285, 1204, 1146, 1099, 1026, 979, 843 cm^{-1}; ^1H and ^{13}C NMR data are shown in Table 2; HRESIMS obsd *m*/*z* 377.1007 $[M + Na]^+$ (calcd for $C_{20}H_{18}O_6Na$, 377.1001).

*Sphenostylisin F (**6**).* Yellow amorphous solid; $[\alpha]_D^{20}$ −6 (*c* 0.1, MeOH); UV (MeOH) λ_{max}/nm (log[ε/M^{-1} cm^{-1}]) 206 (4.70), 247 (4.02), 349 (4.26); IR (film) ν_{max} 3289, 2976, 2927, 1691, 1621, 1581, 1497, 1456, 1368, 1292, 1241, 1152, 1021, 981, 932, 848, 543 cm^{-1}; ^1H and ^{13}C NMR data are shown in Table 2; HRESIMS obsd *m*/*z* 377.0991 $[M + Na]^+$ (calcd for $C_{20}H_{18}O_6Na$, 377.1001).

*Sphenostylisin G (**7**).* Yellow amorphous solid; $[\alpha]_D^{20}$ +9 (*c* 0.1, MeOH); UV (MeOH) λ_{max}/nm (log[ε/M^{-1} cm^{-1}]) 206 (4.70), 248 (3.99), 350 (4.27); IR (film) ν_{max} 3273, 2974, 1689, 1616, 1578, 1509, 1461, 1366, 1291, 1232, 1165, 1102, 1022, 980, 846, 551 cm^{-1}; ^1H and ^{13}C NMR data are shown in Table 2; HRESIMS obsd *m*/*z* 377.0993 $[M + Na]^+$ (calcd for $C_{20}H_{18}O_6Na$, 377.1001).

*Sphenostylisin H (**8**).* Yellow amorphous solid; $[\alpha]_D^{20}$ −5 (*c* 0.1, MeOH); UV (MeOH) λ_{max}/nm (log[ε/M^{-1} cm^{-1}]) 221 (4.34), 250 (4.24), 288 (4.10); IR (film) ν_{max} 3354, 2934, 1615, 1575, 1464, 1374, 1268, 1116, 1024, 847 cm^{-1}; ^1H and ^{13}C NMR data are shown in Table 2; HRESIMS obsd *m*/*z* 377.0995 $[M + Na]^+$ (calcd for $C_{20}H_{18}O_6Na$, 377.1001).

*Sphenostylisin I (**9**).* Colorless resin; $[\alpha]_D^{20}$ −3 (*c* 0.1, MeOH); UV (MeOH) λ_{max}/nm (log[ε/M^{-1} cm^{-1}]) 210 (4.24), 224 (sh, 4.01), 280 (3.90), 316 (3.73); IR (film) ν_{max} 3310, 2962, 2933, 1625, 1497, 1445, 1363, 1293, 1232, 1143, 1024, 845, 802 cm^{-1}; ^1H and ^{13}C NMR data are shown in Table 3; HRESIMS obsd *m*/*z* 367.1151 $[M + Na]^+$ (calcd for $C_{19}H_{20}O_6Na$, 367.1158).

*Sphenostylisin J (**10**).* Colorless resin; $[\alpha]_D^{20}$ −4 (*c* 0.1, MeOH); UV (MeOH) λ_{max}/nm (log[ε/M^{-1} cm^{-1}]) 212 (4.30), 224 (sh, 4.09), 279 (4.04), 316 (3.85); IR (film) ν_{max} 3288, 2971, 2939, 1625, 1506, 1446, 1359, 1290, 1232, 1179, 1140, 1105, 1021, 927, 848, 801 cm^{-1}; ^1H and ^{13}C NMR data are shown in Table 3; HRESIMS obsd *m*/*z* 367.1153 $[M + Na]^+$ (calcd for $C_{19}H_{20}O_6Na$, 367.1158).

*Sphenostylisin K (**11**).* Colorless resin; $[\alpha]_D^{20}$ −4 (*c* 0.1, MeOH); UV (MeOH) λ_{max}/nm (log[ε/M^{-1} cm^{-1}]) 211 (4.28), 224 (sh, 4.05), 279 (3.96), 316 (3.81); IR (film) ν_{max} 3197, 2968, 2924, 1624, 1507, 1456, 1237, 1177, 1135, 1023, 999, 849 cm^{-1}; ^1H and ^{13}C NMR data are shown in Table 3; HRESIMS obsd *m*/*z* 367.1149 $[M + Na]^+$ (calcd for $C_{19}H_{20}O_6Na$, 367.1158).

Cyclization Reaction of 9 To Form a 2-Arylbenzofuran Skeleton. To a 5 mL round-bottom flask under nitrogen containing **9** (1.0 mg) were added freshly dried and degassed THF (1 mL), Amberlyst 15 resin (3.9 mg), and freshly dried, powdered 4 Å molecular sieves (3.0 mg). After the mixture was stirred at 50 °C for 9 h under a N_2 atmosphere, TLC (7:1 $CHCl_3$–MeOH) indicated the reaction to be complete. The crude reaction solution was evaporated in vacuo and dissolved in CD_3OD for ^1H NMR spectroscopic measurements, which showed the presence of extra singlets at δ_H 7.02 and 7.20 (H-3) in the products and the disappearance of the H-8 signal (δ_H 4.07) of the starting material (**9**). This indicated that the cyclization of **9** between OH-2′ and the carbonyl carbon (C-7) was successful, generating the expected 2-arylbenzofuran skeleton (Figure S12a in the Supporting Information). The product mixture was then purified by HPLC on a semipreparative C_{18} column (5 μm, 150 mm × 10 mm i.d.) using a MeOH–H_2O gradient (50–70% MeOH from 0 to 40 min and 70–100% MeOH from 40 to 50 min; flow rate 4.0 mL/min) to be separated as three major peaks (peak 1, t_R = 8.1 min; peak 2, t_R = 22.8 min; peak 3, t_R = 31.0 min). The UV absorbances of peaks 1–3 were recorded using a PDA detector coupled with the HPLC, and the characteristic UV spectra of peaks 2 (λ_{max} 218, 295 sh, 320, and 341 nm) and 3 (λ_{max} 218, 295 sh, 323, and 343 nm) (Figure S12b in the Supporting Information) were comparable to those of the previously reported 2-arylbenzofuran derivatives,[31,32] which further supported the generation of the expected 2-arylbenzofuran skeleton in the reaction. Because of the very small amount of **9** available for the reaction, the amount of the products purified from peaks 2 and 3 was not enough for full structural characterization via NMR spectroscopy.

Evaluation of Hydroxyl Radical-Scavenging Activity. Hydroxyl radical-scavenging activities were evaluated according to a method described previously[33,34] (protocol S1 in the Supporting Information).

Evaluation of Quinone Reductase-Inducing Activity. The potential QR-inducing activities of the extracts, fractions, and pure isolates were assayed as described previously[34,35] (protocol S2 in the Supporting Information).

Evaluation of NF-κB Inhibition Activity. The NF-κB assays were carried out according to an established protocol[36] (protocol S3 in the Supporting Information).

Evaluation of Cytotoxicity. The cytotoxic activities of the pure compounds isolated were assayed on the basis of a method described previously[37,38] (protocol S4 in the Supporting Information).

dx.doi.org/10.1021/jo401573h | J. Org. Chem. 2013, 78, 10166–10177

Conformational Analysis of 1 and 3 Using the LigPrep/ConfGen Software Suite. The 2D SDF file format was converted to a 3D format using the LigPrep program (version 2.5; Schrödinger LLC, New York, NY). LigPrep accounts for the different tautomeric and stereoisomeric states of the compounds as well as a low-energy ring conformation sampling. Possible ionization states of the compounds at pH 7 ± 2 were generated using the Epic module. Energy minimization was performed using the OPLS2005 force field to obtain geometry-optimized 3D coordinates. The output of LigPrep was passed on for further conformational sampling utilizing a ConfGen advanced module (version 2.3; Schrödinger LLC). Energy minimization calculations also used the OPLS2005 force field. A GB/SA solvation model of water was used with a setting of constant dielectric for the electrostatic treatment and 1.0 for the dielectric constant. A maximum of 100 steps of truncated Newton conjugate gradient (TNCG) minimizations proceeded until the rms force dropped below a specified threshold (0.05 kcal mol^{-1} $Å^{-1}$). Finally, a rapid search mode was implemented to produce conformers of compounds **1** and **3**.

■ ASSOCIATED CONTENT

Supporting Information

^{1}H, ^{13}C, ^{13}C DEPT 135, $^{1}H-^{1}H$ COSY, HSQC, and HMBC NMR spectra as well as tables of NMR data for compounds **1**−**11**; UV, ECD, and NOESY spectra for compound **3**; ^{1}H NMR spectra and HPLC separation chromatogram of the crude reaction solution for the reaction shown in Scheme 1; HRESIMS data for compounds **1**−**11**; ESIMS/MS data for compounds **1**−**3**; tandem MS fragmentation scheme for compound **3**; plausible biogenetic relationships among compounds **1**−**11**; and protocols of hydroxyl radical-scavenging, QR-inducing, NF-κB inhibition, and cytotoxicity assays. This material is available free of charge via the Internet at http://pubs.acs.org.

■ AUTHOR INFORMATION

Corresponding Author

*Tel: 1-(614) 247-8094. Fax: 1-(614) 247-8119. E-mail: kinghorn.4@osu.edu.

Notes

The authors declare no competing financial interest.

[#]N.R.F.: Deceased September 11, 2011.

■ ACKNOWLEDGMENTS

We acknowledge financial support for this work from Projects U01/U19 CA52956 and P01 CA125066 funded by NCI/NIH. We thank Mr. John W. Fowble (College of Pharmacy, The Ohio State University) for facilitating the acquisition of NMR data. Mr. Mark Apsega of the Mass Spectrometry & Proteomics Facility at The Ohio State University is acknowledged for MS training.

■ REFERENCES

(1) Sohni, Y. R.; Mutangadura-Mhlanga, T.; Kale, P. G. *Mutat. Res.* **1994**, *322*, 133−140.
(2) Malaisse, F.; Parent, G. *Ecol. Food Nutr.* **1985**, *18*, 43−82.
(3) Gunzinger, J.; Msonthi, J. D.; Hostettmann, K. *Helv. Chim. Acta* **1988**, *71*, 72−76.
(4) Cuendet, M.; Oteham, C. P.; Moon, R. C.; Pezzuto, J. M. *J. Nat. Prod.* **2006**, *69*, 460−463.
(5) Sarkar, F. H.; Li, Y. *Front. Biosci.* **2008**, *13*, 2950−2959.
(6) Hatano, T.; Aga, Y.; Shintani, Y.; Ito, H.; Okuda, T.; Yoshida, T. *Phytochemistry* **2000**, *55*, 959−963.
(7) Yang, Y.; Zhang, T.; Xiao, L.; Yang, L.; Chen, R. *Fitoterapia* **2010**, *81*, 614−616.
(8) Cuyckens, F.; Claeys, M. *J. Mass Spectrom.* **2004**, *39*, 1−15.
(9) Jaiswal, R.; Jayasinghe, L.; Kuhnert, N. *J. Mass Spectrom.* **2012**, *47*, 502−515.
(10) Li, H. J.; Deinzer, M. L. *Anal. Chem.* **2007**, *79*, 1739−1748.
(11) Pan, L.; Matthew, S.; Lantvit, D. D.; Zhang, X.; Ninh, T. N.; Chai, H.; Carcache de Blanco, E. J.; Soejarto, D. D.; Swanson, S. M.; Kinghorn, A. D. *J. Nat. Prod.* **2011**, *74*, 2193−2199.
(12) Bezuidenhoudt, B. C. B.; Brandt, E. V.; Steenkamp, J. A.; Roux, D. G.; Ferreira, D. *J. Chem. Soc., Perkin Trans. 1* **1988**, 1227−1235.
(13) Rohwer, M. B.; van Heerden, P. S.; Brandt, E. V.; Bezuidenhoudt, B. C. B.; Ferreira, D. *J. Chem. Soc., Perkin Trans. 1* **1999**, 3367−3374.
(14) Rufer, C. E.; Glatt, H.; Kulling, S. E. *Drug Metab. Dispos.* **2006**, *34*, 51−60.
(15) Pinheiro, P. F.; Justino, G. C. Structural Analysis of Flavonoids and Related Compounds: A Review of Spectroscopic Applications. In *Phytochemicals: A Global Perspective of Their Role in Nutrition and Health*; Rao, V., Ed.; InTech: Rijeka, Croatia, 2012; pp 42−44.
(16) Slade, D.; Ferreira, D.; Marais, J. P. *Phytochemistry* **2005**, *66*, 2177−2215.
(17) Kurosawa, K.; Ollis, W. D.; Redman, B. T.; Sutherland, I. O. *Chem. Commun.* **1968**, 1265−1267.
(18) Kim, M.; Kim, S.; Kim, Y.; Han, J. *Bull. Korean Chem. Soc.* **2009**, *30*, 415−418.
(19) Yoo, H. S.; Lee, J. S.; Kim, C. Y.; Kim, J. *Arch. Pharm. Res.* **2004**, *27*, 544−546.
(20) Kiuchi, F.; Chen, X.; Tsuda, Y. *Heterocycles* **1990**, *31*, 629−636.
(21) Zeng, J. F.; Zhu, D. Y. *Acta Bot. Sin.* **1999**, *41*, 997−1001.
(22) Dewick, P. M. In *The Flavonoids: Advances in Research since 1986*; Harborne, J. B., Ed.; Chapman and Hall: London, 1994; pp 195−206.
(23) Ko, H. H.; Weng, J. R.; Tsao, L. T.; Yen, M. H.; Wang, J. P.; Lin, C. N. *Bioorg. Med. Chem. Lett.* **2004**, *14*, 1011−1014.
(24) Boonnak, N.; Khamthip, A.; Karalai, C.; Chantrapromma, S.; Ponglimanont, C.; Kanjana-Opas, A.; Tewtrakul, S.; Chantrapromma, K.; Fun, H. K.; Kato, S. *Aust. J. Chem.* **2010**, *63*, 1550−1556.
(25) Whalley, W. B.; Lloyd, G. *J. Chem. Soc.* **1956**, 3213−3224.
(26) Li, L.; Cheng, X. F.; Leshkevich, J.; Umezawa, T.; Harding, S. A.; Chiang, V. L. *Plant Cell* **2001**, *13*, 1567−1586.
(27) Alphey, M. S.; Yu, W.; Byres, E.; Li, D.; Hunter, W. N. *J. Biol. Chem.* **2005**, *280*, 3068−3077.
(28) Wei, Y.; Lin, M.; Oliver, D. J.; Schnable, P. S. *BMC Biochem.* **2009**, *10*, 7.
(29) Diller, D. J.; Merz, K. M., Jr. *J. Comput.-Aided Mol. Des.* **2002**, *16*, 105−112.
(30) Perola, E.; Charifson, P. S. *J. Med. Chem.* **2004**, *47*, 2499−2510.
(31) Halabalaki, M.; Aligiannis, N.; Papoutsi, Z.; Mitakou, S.; Moutsatsou, P.; Sekeris, C.; Skaltsounis, A. L. *J. Nat. Prod.* **2000**, *63*, 1672−1674.
(32) Yenesew, A.; Midiwo, J. O.; Guchu, S. M.; Heydenreich, M.; Peter, M. G. *Phytochemistry* **2002**, *59*, 337−341.
(33) LeBel, C. P.; Ischiropoulos, H.; Bondy, S. C. *Chem. Res. Toxicol.* **1992**, *5*, 227−231.
(34) Li, J.; Deng, Y.; Yuan, C.; Pan, L.; Chai, H.; Keller, W. J.; Kinghorn, A. D. *J. Agric. Food Chem.* **2012**, *60*, 11551−11559.
(35) Su, B. N.; Jung, P. E.; Vigo, J. S.; Graham, J. G.; Cabieses, F.; Fong, H. H.; Pezzuto, J. M.; Kinghorn, A. D. *Phytochemistry* **2003**, *63*, 335−341.
(36) Deng, Y.; Balunas, M. J.; Kim, J. A.; Lantvit, D. D.; Chin, Y. W.; Chai, H.; Sugiarso, S.; Kardono, L. B.; Fong, H. H.; Pezzuto, J. M.; Swanson, S. M.; Carcache de Blanco, E. J.; Kinghorn, A. D. *J. Nat. Prod.* **2009**, *72*, 1165−1169.
(37) Pan, L.; Kardono, L. B.; Riswan, S.; Chai, H.; Carcache de Blanco, E. J.; Pannell, C. M.; Soejarto, D. D.; McCloud, T. G.; Newman, D. J.; Kinghorn, A. D. *J. Nat. Prod.* **2010**, *73*, 1873−1878.
(38) Pan, L.; Acuna, U. M.; Li, J.; Jena, N.; Ninh, T. N.; Pannell, C. M.; Chai, H.; Fuchs, J. R.; Carcache de Blanco, E. J.; Soejarto, D. D.; Kinghorn, A. D. *J. Nat. Prod.* **2013**, *76*, 394−404.